

# Ground-state selection and spin-liquid behaviour in the classical Heisenberg model on the breathing pyrochlore lattice

Owen Benton\* and Nic Shannon

*Okinawa Institute of Science and Technology Graduate University, Onna-son, Okinawa 904-0395, Japan*

Magnetic pyrochlore oxides, including the spin ice materials, have proved to be a rich field for the study of geometrical frustration in 3 dimensions. Recently, a new family of magnetic oxides has been synthesised in which the half of the tetrahedra in the pyrochlore lattice are inflated relative to the other half, making an alternating array of small and large tetrahedra. These “breathing pyrochlore” materials such as  $\text{LiGaCr}_4\text{O}_8$ ,  $\text{LiInCr}_4\text{O}_8$  and  $\text{Ba}_3\text{Yb}_2\text{Zn}_5\text{O}_{11}$  provide new opportunities in the study of frustrated magnetism. Here we provide an analytic theory for the ground state phase diagram and spin correlations for the minimal model of magnetism in breathing pyrochlores: a classical nearest neighbour Heisenberg model with different exchange coefficients for the two species of tetrahedra. We find that the phase diagram comprises a Coulombic spin liquid phase, a conventional ferromagnetic phase and an unusual antiferromagnetic phase with lines of soft modes in reciprocal space, stabilised by an order-by-disorder mechanism. We obtain a theory of the spin correlations in this model using the Self Consistent Gaussian Approximation (SCGA) which enables us to discuss the development of correlations in breathing pyrochlores as a function of temperature, and we quantitatively characterise the thermal crossover from the limit of isolated tetrahedra to the strongly correlated limit of the problem. We compare the results of our analysis with the results of recent neutron scattering experiments on  $\text{LiInCr}_4\text{O}_8$ .

## 1. Introduction

Systems exhibiting geometrical frustration have proved over recent years to be fertile ground for the discovery of novel emergent phenomena.<sup>1,2</sup> Amongst frustrated magnetic systems there are now several known materials whose low temperature physics displays novel collective behaviour which cannot be understood using the usual Landau picture, based on broken symmetries.<sup>3–8</sup>

At the forefront of the research interest in these systems has been the study of magnetism on the pyrochlore lattice<sup>9</sup> – a network of corner sharing tetrahedra. Nearest neighbour antiferromagnetic coupling between spins on this lattice fails to select a unique ordered state and leads to an exponentially large ground state manifold.<sup>10–12</sup> This results in the formation of a classical spin liquid with extensive residual entropy and algebraically decaying spin correlations.<sup>13,14</sup> The ground state manifold of this spin liquid is defined by a flux conservation law  $\nabla \cdot \mathbf{B} = 0$  and the excitations which violate this law are deconfined “charges” which interact via an emergent Coulomb law. For this reason, this spin liquid is known as a “Coulombic spin liquid”.

The classical Coulomb spin liquid finds realization in several experimental systems. The spin ice materials  $\text{R}_2\text{M}_2\text{O}_7$  ( $\text{R}=\text{Ho}, \text{Dy}; \text{M}=\text{Ti}, \text{Sn}$ ) at low temperature are famous examples of Coulomb liquids of Ising spins.<sup>15</sup> Meanwhile, the chromium spinels  $\text{MCr}_2\text{O}_4$  ( $\text{M}=\text{Zn}, \text{Cd}, \text{Hg}$ ) can be understood in terms of a Coulomb liquid of vector spins interacting with fluctuations of the lattice. As a consequence these materials have emerged as canonical examples of the phenomenon of “order-by-distortion” in which magnetic frustration is relieved by a structural transition.<sup>16–19</sup> Calculations based on a classical effective model for the spins with coupling to the lattice predict a rich phase diagram in an applied magnetic field<sup>20–24</sup> which was observed in a series of remarkable experiments at fields up to 600T.<sup>25–29</sup>

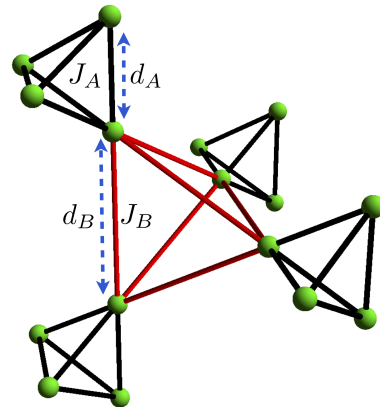


**Fig. 1.** (Color online) The breathing pyrochlore lattice. Like the pyrochlore lattice, the breathing pyrochlore lattice is composed of corner-sharing tetrahedra. However, in the breathing pyrochlore lattice these tetrahedra alternate in size. The spins reside at the vertices of this lattice. The two species of tetrahedra (here labelled ‘A’ and ‘B’, colored black and red) have different bond lengths  $d_A$  and  $d_B$  and different exchange coefficients  $J_A$  and  $J_B$ .

Recently, a new class of magnetic materials has been synthesised which promises an interesting variation on this picture.<sup>30–32,34</sup> In the spinels  $\text{LiInCr}_4\text{O}_8$  and  $\text{LiGaCr}_4\text{O}_8$ <sup>30–33</sup> the  $\text{Cr}^{3+}$  ions, carrying spin  $S = \frac{3}{2}$ , reside on a “breathing” pyrochlore lattice depicted in Fig. 1. In this lattice the tetrahedra of the pyrochlore lattice are alternately small and large, with the consequence that the two sets of tetrahedra have different exchange coefficients. Similarly, in the effective  $S = \frac{1}{2}$  magnet,  $\text{Ba}_3\text{Yb}_2\text{Zn}_5\text{O}_{11}$ , the magnetic  $\text{Yb}^{3+}$  ions reside on a breathing pyrochlore lattice.<sup>34</sup>

As with Cr spinels, these oxide materials have antiferromagnetic nearest-neighbour exchange interactions.<sup>30</sup> However this interaction has contributions from both direct and indirect exchange, with opposite sign, and is very sensitive

\*owen.benton@oist.jp

small changes in bond angles or distances<sup>35,36</sup>. As a result, there is a very real possibility that breathing pyrochlores based on larger anions, such as S or Se, might have ferromagnetic interactions, in at least one of the two sets of tetrahedra.

Theoretical studies of the pyrochlore magnets with unequal exchange interactions on the two species of tetrahedra have concentrated on antiferromagnetic interactions, in the quantum limit  $S = 1/2$ , as a route to understanding the  $S = 1/2$  Heisenberg model on a pyrochlore lattice.<sup>37–40</sup> Performing perturbation theory about the limit of independent independent tetrahedra, Harris *et al.*<sup>37</sup> and Tsunetsugu<sup>40</sup> have explored the possibility of a novel dimerized ground state. Meanwhile Canals and Lacroix,<sup>38,39</sup> considered the possibility of a quantum spin liquid. At present, there is no established study of the Heisenberg model on the breathing pyrochlore lattice in the presence of ferromagnetic interactions, or treatment of spin correlations within the high-temperature paramagnetic phase. The recent synthesis of breathing pyrochlore magnets makes this a pressing issue.

In this article we provide a comprehensive treatment of the ground state phase diagram and spin correlations of the nearest neighbour Heisenberg model on the breathing pyrochlore lattice, for all signs and ratios of exchange couplings. The classical treatment should be particularly relevant for the relatively large-spin  $S = \frac{3}{2}$ ,  $\text{Cr}^{3+}$  systems, in the temperature regime above the structural transitions which are observed in  $\text{LiInCr}_4\text{O}_8$  at 15.9 K and  $\text{LiGaCr}_4\text{O}_8$  at 13.8 K.<sup>30–33</sup>

We find that the nature of the classical ground state depends only the signs of the two exchange coefficients associated with the two species of tetrahedra, not on their relative magnitudes. Where both exchange coefficients are antiferromagnetic the system enters a Coulomb phase at low temperature. Where both exchange coefficients are ferromagnetic the system orders into a simple ferromagnetic phase. Where the exchange coefficients differ in sign, the classical ground state manifold has a degeneracy of  $O(L)$ , where  $L$  is the linear dimension of the system, with antiferromagnetic [001] planes becoming effectively decoupled from one another. This degeneracy is then susceptible to being lifted by fluctuations, stabilising antiferromagnetic order, meaning that this region of the phase diagram combines the properties of dimensional reduction and order-by-disorder noted in other pyrochlore magnets.<sup>41–45</sup> By using the Self Consistent Gaussian Approximation (SCGA)<sup>46–49</sup> we are then able to calculate the behaviour of the spin correlations as a function of the exchange parameters and temperature.

The article is structured as follows:

In Section 2 we obtain the phase diagram of the classical Heisenberg model on the breathing pyrochlore lattice.

In Section 3 we discuss the case of ferromagnetic coupling. We use the SCGA to show the temperature development of the spin correlations and quantify the thermal crossover from isolated tetrahedra to long range correlations by deriving equations for the temperature dependence of the ferromagnetic correlation length.

In Section 4 we discuss the case of exchange parameters with differing signs. We show that the degenerate zero-energy modes which occur in this case lead to a “square ring” structure observable in the neutron scattering response.

In Section 5 we discuss the case of antiferromagnetic cou-

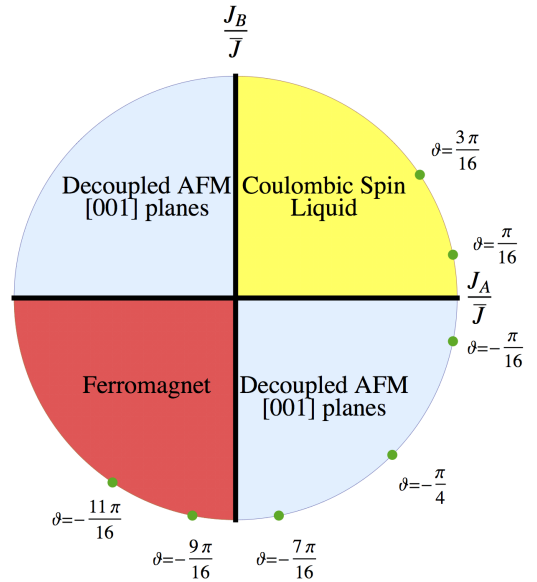


**Fig. 2.** (Color online) Classical ground state phase diagram of the breathing pyrochlore lattice Heisenberg model [Eq. (1)]. The ground state manifold is determined by the signs of the two couplings  $J_A$  and  $J_B$ . Where both couplings are ferromagnetic than the ground state is a simple collinear ferromagnet. Where both couplings are antiferromagnetic the system enters a macroscopically degenerate Coulomb phase, in which the ground state manifold contains all states where every tetrahedron has vanishing magnetisation. If  $J_A$  and  $J_B$  have opposite signs than the set of classical ground states is described by decoupled [001] planes and has a degeneracy  $O(L)$ . This degeneracy will be lifted by the order-by-disorder mechanism. Due to a correspondence with Heisenberg model on the FCC lattice [Eq. (11)] we expect this to favour antiferromagnetic states with ordering vector  $\mathbf{q}_{\text{ord}} = (1, 0, 0)$  [Fig. 3]. The green points indicate the parameter sets for which we plot the spin correlation functions in Figs. 4–9.

pling which leads to a Coulombic spin liquid at low temperature. We show how the algebraic correlations of the spin liquid emerge out of the short range, single tetrahedron, correlations with decreasing temperature.

In Section 6 we conclude with a summary of our results and a comparison of our predictions with the results of neutron scattering experiments on the breathing pyrochlore  $\text{LiInCr}_4\text{O}_8$ .<sup>32</sup>

## 2. Ground state phase diagram

We consider the Heisenberg Hamiltonian on the breathing pyrochlore lattice

$$\mathcal{H}_{\text{breathing}} = J_A \sum_{\langle ij \rangle_A} \mathbf{S}_i \cdot \mathbf{S}_j + J_B \sum_{\langle ij \rangle_B} \mathbf{S}_i \cdot \mathbf{S}_j \quad (1)$$

The two terms in Eq. (1) correspond to the two sets of tetrahedra on the pyrochlore lattice, which we label  $A$  and  $B$  [cf. Fig. 1]. Every bond of the lattice belongs uniquely to one tetrahedron and is associated with an exchange coupling  $J_A$  or  $J_B$  depending on which set of tetrahedra it belongs to, as illustrated in Fig. 1.

The classical ground state phase diagram of Eq. (1) is shown in Fig. 2. As is commonplace for two parameter models, we can re-express the exchange coefficients in terms of an overall energy scale  $\bar{J}$  and an angle  $\vartheta$ :

$$J_A = \bar{J} \cos(\vartheta), \quad J_B = \bar{J} \sin(\vartheta) \quad (2)$$

There are three distinct phases on the phase diagram:

- (1) For  $0 < \vartheta < \frac{\pi}{2}$  ( $J_A > 0, J_B > 0$ ) the ground state manifold contains all states where the magnetisation of every tetrahedron in the lattice vanishes and the system is in a Coulomb phase at low temperature.
- (2) For  $-\pi < \vartheta < -\frac{\pi}{2}$  ( $J_A < 0, J_B < 0$ ) the ground state is a collinear ferromagnetic state
- (3) For  $-\frac{\pi}{2} < \vartheta < 0$  ( $J_A > 0, J_B < 0$ ) or  $\frac{\pi}{2} < \vartheta < \pi$  ( $J_A < 0, J_B > 0$ ) the ground state is comprises an  $O(L)$  set of antiferromagnetic states with wavevectors of the form of  $\mathbf{q}_\delta = (\delta, 0, 1)$  (and those related by symmetry). This ground state manifold may be mapped directly to the classical ground state manifold of the nearest neighbour FCC antiferromagnet,<sup>50,51</sup> as we shall show below.

The phase diagram shown in Fig. 2 may be derived using the following argument. As in the case of the Heisenberg model on the ordinary (non-breathing) pyrochlore lattice, the Hamiltonian [Eq. (1)] can be rewritten as a function only of the magnetisation of each tetrahedron. We define, for a tetrahedron  $t$ , the magnetisation density

$$\mathbf{m}_t = \frac{1}{4S} \sum_{i \in t} \mathbf{S}_i \quad (3)$$

where the sum runs over the four spins at the vertices of tetrahedron  $t$ . Eq. (1) can then be rewritten solely in terms of the variables  $\mathbf{m}_t$

$$\mathcal{H}_{\text{breathing}} = 8J_A S^2 \sum_{t \in A} \mathbf{m}_t^2 + 8J_B S^2 \sum_{t \in B} \mathbf{m}_t^2 - \frac{(J_A + J_B)}{2} N S^2 \quad (4)$$

It is clear from Eq. (4) that when  $J_A$  and  $J_B$  are both anti-ferromagnetic, any state where

$$\mathbf{m}_t = \begin{pmatrix} 0 \\ 0 \\ 0 \end{pmatrix} \quad \forall t \quad (5)$$

is a classical ground state. This constraint gives rise to a Coulomb phase.<sup>14</sup>

It is similarly clear from Eq. (4) that when  $J_A$  and  $J_B$  are both ferromagnetic, the ground state is obtained when every tetrahedron has a maximal value of  $\mathbf{m}_t^2$

$$\mathbf{m}_t^2 = 1 \quad \forall t \quad (6)$$

This condition is only satisfied by collinear ferromagnetic states.

Where the signs of  $J_A$  and  $J_B$  differ we can see from Eq. (4) that the condition to be in a ground state is that all ferromagnetic tetrahedra have aligned spins but the intervening antiferromagnetic tetrahedra have vanishing magnetisation. Taking, without loss of generality

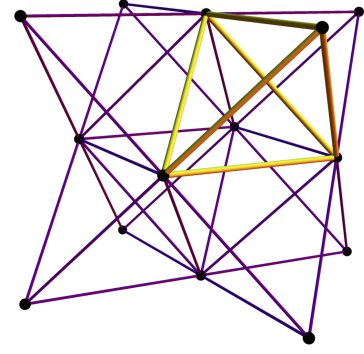
$$J_A > 0, \quad J_B < 0$$

we require

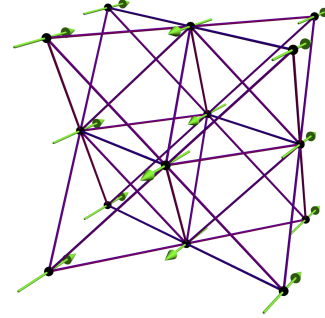
$$\mathbf{m}_t^2 = 0 \quad \forall t \in A \quad (7)$$

$$\mathbf{m}_t^2 = 1 \quad \forall t \in B \quad (8)$$

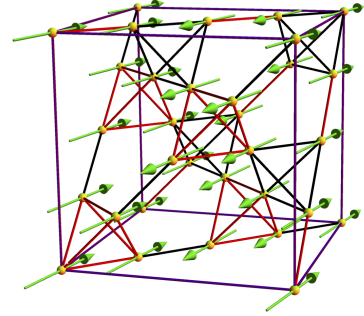
These constraints lead to an equivalent classical ground state manifold to the nearest neighbour Heisenberg model on the FCC lattice. We can see this by considering the Hamilto-



(a) The FCC lattice as a network of edge-sharing tetrahedra



(b) The (100) state on the FCC lattice



(c) The (100) state on the breathing pyrochlore lattice

**Fig. 3.** (Color online). The mapping to the FCC antiferromagnet when  $J_A$  and  $J_B$  have opposite signs and the resulting antiferromagnetic order. Each sublattice of tetrahedra ( $A$  and  $B$ ) of the breathing pyrochlore lattice forms an FCC lattice, which can be viewed as a network of edge sharing tetrahedra, as seen in A. Where the exchange coefficients  $J_A$  and  $J_B$  differ in sign, the classical ground state manifold of Eq. (1) is the same as the ground state manifold of the nearest neighbour antiferromagnet on the FCC lattice, with each ferromagnetic tetrahedron of the breathing pyrochlore model corresponding to a single spin of the FCC model. This model has an  $O(L)$  set of ground states with fluctuations favouring collinear states with ordering wavevector  $\mathbf{q}_{\text{ord}} = (1, 0, 0)$  (and states related by global symmetries). As a result, the FCC model orders into the configuration shown in (b). Since the two models have an exactly corresponding structure of soft modes, the order by disorder mechanism should favour the analogous state on the breathing pyrochlore lattice [shown in (c)] when  $J_A$  and  $J_B$  have opposite signs.

nian [Eq. (1)] restricted to the subspace where Eq. (8) is perfectly obeyed. Since this fixes the exchange energy of all the  $B$  tetrahedra, the Hamiltonian within this set of configurations

becomes

$$\mathcal{H}_{\text{breathing}}^{\text{FM-B}} = 8J_A S^2 \sum_{t \in A} \mathbf{m}_t^2 + \frac{(3J_B - J_A)}{2} N S^2 \quad (9)$$

Since all the spins on each  $B$  tetrahedron are ferromagnetically aligned the magnetisation of the  $A$  tetrahedra is determined uniquely by the total magnetisation of the four surrounding  $B$  tetrahedra

$$\mathbf{m}_{t_A} = \frac{1}{4} \sum_{t_B \in \text{n.n. } t_A} \mathbf{m}_{t_B}. \quad (10)$$

Inserting Eq. (10) into Eq. (9) and using Eq. (8) we obtain a nearest neighbour antiferromagnetic interaction between  $A$  tetrahedra.

$$\mathcal{H}_{\text{breathing}}^{\text{FM-B}} = J_A S^2 \sum_{\langle t_B t_B' \rangle} \mathbf{m}_{t_B} \cdot \mathbf{m}_{t_B'} + \frac{3J_B}{2} N S^2 \quad (11)$$

where the sum  $\sum_{\langle t_B t_B' \rangle}$  runs over nearest neighbours of the FCC lattice of  $B$  tetrahedra.

The FCC lattice may be depicted as a network of *edge-sharing* tetrahedra as shown in Fig. 3(a). A ground state for the nearest neighbour antiferromagnet on this lattice is obtained when each of these edge-sharing tetrahedra have vanishing magnetisation. Under the mapping from the breathing pyrochlore model [Eq. (4)] to the FCC model [Eq. (11)] this requirement is equivalent to Eq. (7).

One ground state configuration of Eq. (11) is depicted in Fig. 3(b). This is an antiferromagnetic state with ordering wavevector  $\mathbf{q}_{\text{ord}} = (1, 0, 0)$ . The corresponding state on the breathing pyrochlore lattice is depicted in Fig. 3(c) and one can readily verify that it satisfies Eqs.(7)-(8).

Further ground states can be generated from the configuration in Fig. 3(b), by taking (e.g.) [001] planes of spins and rotating them with respect to the rest of the lattice. This operation keeps the system in the classical ground state manifold. By generating ground states using these operations we see that the ground state manifold contains states with wavevectors

$$\mathbf{q}_\delta = (1, 0, \delta) \quad (12)$$

(and those wavevectors related to Eq. (12) by lattice symmetries).

From these considerations we can see that states with wavevectors

$$\mathbf{q}_{\text{ord}} = (1, 0, 0) \quad (13)$$

are special because they live at the junctions of the ground state manifold, where two lines of classical ground states (in the case of Eq. (13) those with  $\mathbf{q}_\delta = (1, 0, \delta)$  and  $\mathbf{q}_\delta = (1, \delta, 0)$ ) meet. The resulting freedom to fluctuate for zero energy cost should favour these states for selection via the order-by-disorder mechanism.<sup>12,45</sup>

In the nearest neighbour FCC model it is known that fluctuations do indeed favour states with ordering wavevector  $\mathbf{q}_{\text{ord}} = (1, 0, 0)$  (referred to in the literature as Type I AFM states).<sup>50,51</sup> This entropic preference for states with  $\mathbf{q}_{\text{ord}} = (1, 0, 0)$  results in a first order phase transition into these states.<sup>51</sup>

Since the ground state manifold of the breathing pyrochlore model [Eq. (1)] with  $J_A < 0$ ,  $J_B > 0$  (or equivalently  $J_A > 0$ ,  $J_B < 0$ ) is the same as in the FCC model [Eq. (11)], the

structure of the soft modes is also the same, and it therefore seems reasonable to postulate that the ground state selection will also be the same.

In the limit  $|J_A| \gg |J_B|$ , for  $J_A < 0$ ,  $J_B > 0$ , i.e. where the ferromagnetic exchange is much stronger than the antiferromagnetic, fluctuations which are internal to the ferromagnetic tetrahedra will cost a lot of energy and [Eq. (11)] will be a faithful treatment not only of the ground state manifold but also of the low energy fluctuations. Therefore, in this limit at least, the ground state selection must be the same as in the FCC model. Since tuning away from the limit  $|J_A| \gg |J_B|$  does not change the structure of the ground state manifold we make the conjecture that the  $\mathbf{q}_{\text{ord}} = (1, 0, 0)$  state is selected across the whole region where  $J_A$  and  $J_B$  have opposite signs, although this would need to be confirmed by simulation.

In the temperature range above the phase transition, two planes neighbouring [001] planes with short range order at  $\mathbf{q} = (1, 0, 0)$  will become effectively decoupled and fluctuate essentially independently. This gives rise to an apparent dimensional reduction, which will manifest itself as line like features in the structure factor in the paramagnetic phase, in a similar phenomenon to that observed in the paramagnetic phase of the rare earth pyrochlore  $\text{Yb}_2\text{Ti}_2\text{O}_7$ .<sup>41,42,45</sup> We will discuss this point further where we calculate the spin correlations in this region of the phase diagram in Section 4.

### 3. $J_A < 0$ , $J_B < 0$ : ferromagnetic phase

In this Section we analyse the spin correlations where the exchange coefficients  $J_A$  and  $J_B$  are ferromagnetic. Here, and in the following two Sections where we analyse the other regions of the phase diagram, we use the Self Consistent Gaussian Approximation (SCGA) to calculate the spin correlation functions. This approach is known to be qualitatively successful in treating the spin correlations of classical vector spin models on the pyrochlore lattice.<sup>13,46-49</sup>

In this treatment of the spin correlations, the ‘‘hard spin’’ constraint that each vector spin have fixed length

$$\mathbf{S}_i \cdot \mathbf{S}_i = S^2 \quad \forall \quad i \quad (14)$$

is relaxed such that Eq. (14) is satisfied only on average:

$$\langle \mathbf{S}_i \cdot \mathbf{S}_i \rangle = S^2 \quad \forall \quad i \quad (15)$$

Eq. (15) is enforced by means of a Lagrange multiplier  $\lambda$ . Specifically, we write

$$\begin{aligned} \beta \mathcal{H}_{\text{breathing}} &\rightarrow \beta \mathcal{H}_{\text{breathing}}^{\text{SCGA}} \\ &= \beta \mathcal{H}_{\text{breathing}} + (\lambda - \beta \epsilon_0) \sum_i \mathbf{S}_i^2. \end{aligned} \quad (16)$$

Here  $\beta$  is the inverse temperature and

$$\epsilon_0 = \frac{E_0}{N S^2} \quad (17)$$

where  $E_0$  is the ground state energy. In Eq. (16) we have subtracted the constant term  $\epsilon_0 \sum_i \mathbf{S}_i^2$  from the Hamiltonian so that  $\mathcal{H}_{\text{breathing}}^{\text{SCGA}}$  is positive definite as long as  $\lambda > 0$ . This step makes no difference to the results of our analysis, but is mathematically convenient.

We define Fourier transformed variables

$$S_i^\alpha(\mathbf{q}) = \sqrt{\frac{1}{N_{\text{uc}}}} \sum_{\mathbf{r}_i} \exp(-i\mathbf{q} \cdot \mathbf{r}_i) S^\alpha(\mathbf{r}_i) \quad (18)$$

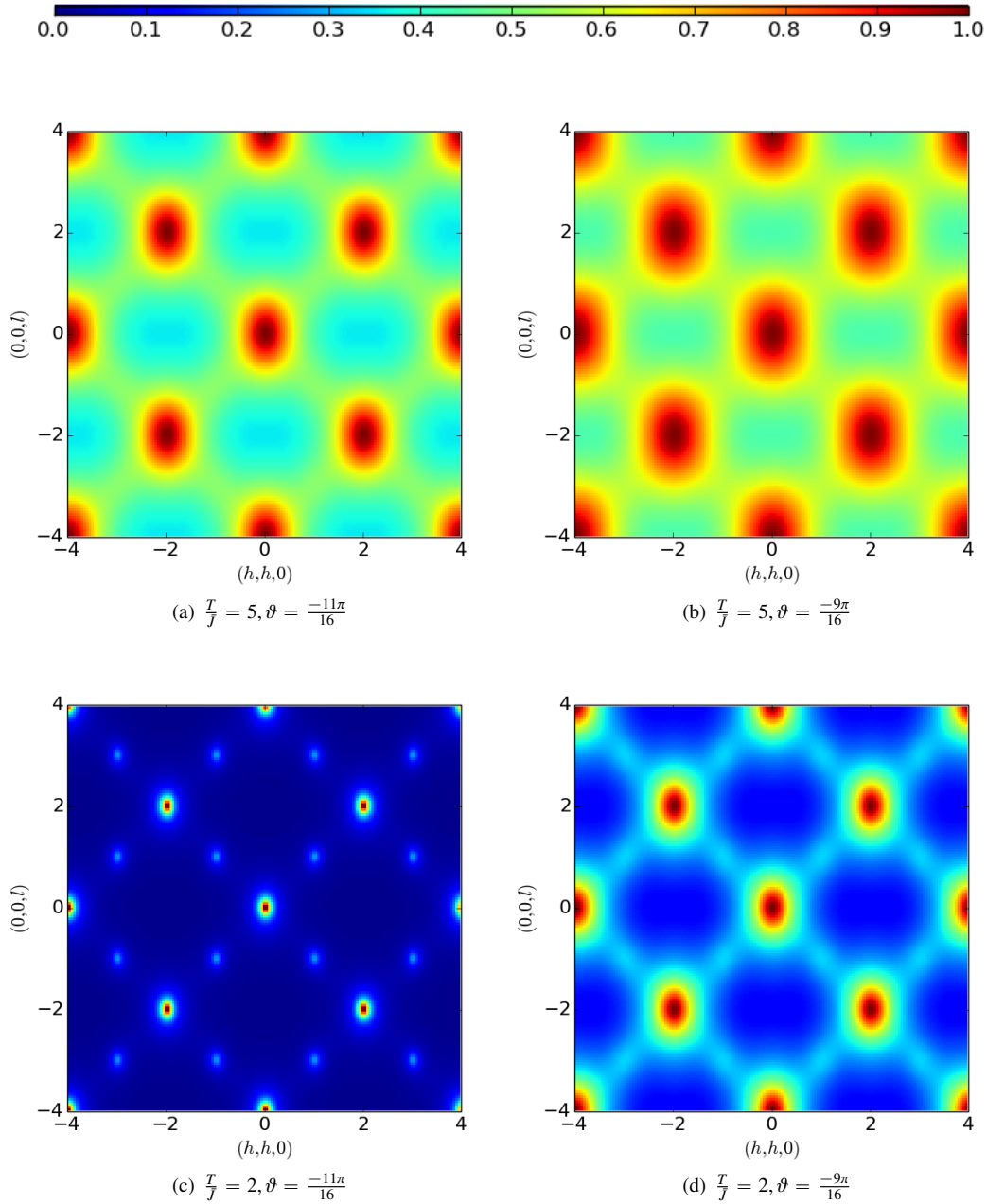


**Fig. 4.** (Color online) Spin structure factor  $\mathcal{S}(\mathbf{q})$  [Eq. (??)] in the Ferromagnetic region of the phase diagram of  $\mathcal{H}_{\text{breathing}}$  [Eq. (1)] for  $\vartheta = \frac{-11\pi}{16}$  (close to the non-breathing limit  $J_A = J_B$ ) and  $\vartheta = \frac{-9\pi}{16}$  (close to the isolated tetrahedron limit  $J_A = 0$ ) [cf. Fig. 2].  $\mathcal{S}(\mathbf{q})$  is calculated from the Self Consistent Gaussian Approximation (SCGA) described at the beginning of Section 3. With decreasing temperature the scattering sharpens around  $\mathbf{q} = (0, 0, 0)$  and other ferromagnetic zone centers. The sharpening is less pronounced at equal temperature for  $\vartheta = \frac{-9\pi}{16}$  because the growth of the correlation length at low temperatures is controlled by the product  $J_A J_B$  which vanishes in the isolated tetrahedron limit [Eqs. (30)-(36)].

where  $\alpha = x, y, z$  indexes the spin components,  $i = 0, 1, 2, 3$  indexes the four sublattices of the breathing pyrochlore lattice and  $\sum_{\mathbf{r}_i}$  runs over all the sites  $\mathbf{r}_i$  belonging to sublattice  $i$ .

Re-writing  $\beta\mathcal{H}_{\text{breathing}}^{\text{SCGA}}$  [Eq. (16)] in terms of  $S_i^\alpha(\mathbf{q})$  [Eq. (18)] we obtain

$$\beta\mathcal{H}_{\text{breathing}}^{\text{SCGA}} = \frac{1}{2} \sum_{\mathbf{q}} \sum_{\alpha} \sum_{ij} S_i^\alpha(-\mathbf{q}) \mathcal{M}_{ij}(\mathbf{q}) S_j^\alpha(\mathbf{q}). \quad (19)$$

The components of  $4 \times 4$  matrix  $\mathcal{M}_{ij}(\mathbf{q})$  are

$$\begin{aligned} \mathcal{M}_{ij}(\mathbf{q}) &= 2\delta_{ij}(\lambda - \beta\epsilon_0) + \mathcal{A}_{ij} \left[ J_A \exp\left(i\frac{d_A}{\sqrt{8}}(\mathbf{e}_i - \mathbf{e}_j)\right) \right. \\ &\quad \left. + J_B \exp\left(-i\frac{d_B}{\sqrt{8}}(\mathbf{e}_i - \mathbf{e}_j)\right) \right] \end{aligned} \quad (20)$$

where

$$\mathcal{A} = \begin{pmatrix} 0 & 1 & 1 & 1 \\ 1 & 0 & 1 & 1 \\ 1 & 1 & 0 & 1 \\ 1 & 1 & 1 & 0 \end{pmatrix} \quad (21)$$

$$\begin{aligned} \mathbf{e}_0 &= (1, 1, 1) & \mathbf{e}_1 &= (1, -1, -1) \\ \mathbf{e}_2 &= (-1, 1, -1) & \mathbf{e}_3 &= (-1, -1, 1) \end{aligned} \quad (22)$$

and  $d_A, d_B$  are the bond lengths on the  $A$  and  $B$  tetrahedra respectively [Fig. 1].

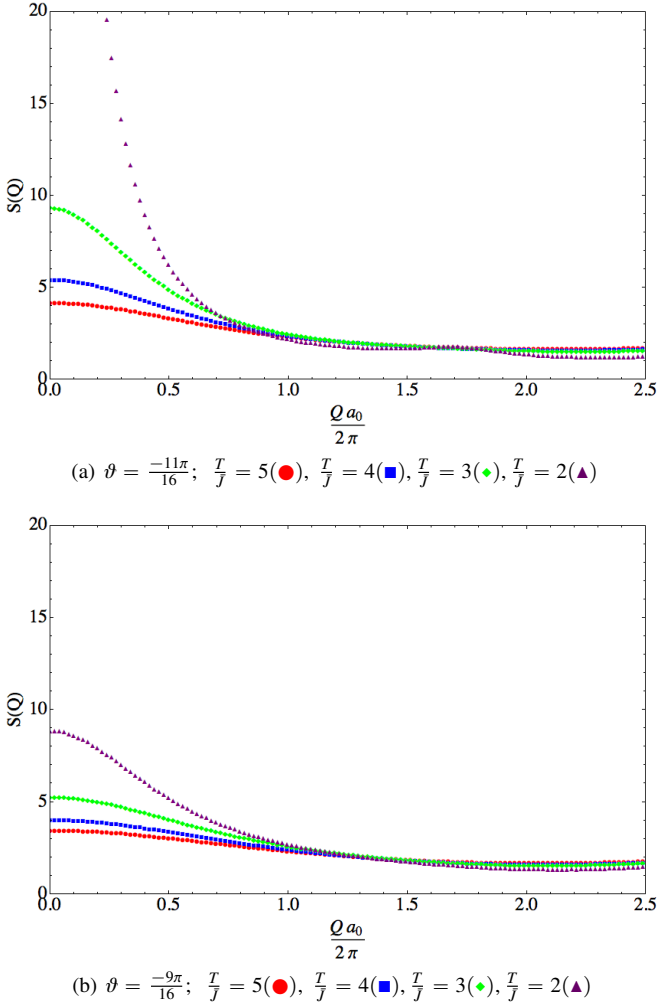


**Fig. 5.** (Color online) Angle integrated structure factor  $S_{\text{pow}}(Q)$  [Eq. (27)] in the ferromagnetic region of the phase diagram [Fig. 2] of  $\mathcal{H}_{\text{breathing}}$  [Eq. (1)]. The structure factor is calculated from the SCGA as described at the beginning of Section 3. Calculation is shown for  $\theta = \frac{-11\pi}{16}$  and  $\theta = \frac{-9\pi}{16}$ . Where the disparity between  $J_A$  and  $J_B$  is greater the ferromagnetic correlations build up more slowly with decreasing temperature.

The partition function within the SCGA is then

$$\mathcal{Z}_{\text{SCGA}} = \int \prod_{\mathbf{q}} \prod_{\alpha} dS^{\alpha}(\mathbf{q}) \exp\left(-\beta \mathcal{H}_{\text{breathing}}^{\text{SCGA}}\right). \quad (23)$$

Since  $\beta \mathcal{H}_{\text{breathing}}^{\text{SCGA}}$  is Gaussian the spin correlation functions within the SCGA are given by

$$\langle S_i^{\mu}(-\mathbf{q}) S_j^{\nu}(\mathbf{q}) \rangle = \delta^{\mu\nu} [\mathcal{M}(\mathbf{q})^{-1}]_{ij}. \quad (24)$$

The Lagrange multiplier  $\lambda$  is then determined self consistently from Eqs. (15) and (24).

The results of this analysis, for ferromagnetic exchange parameters  $J_A, J_B < 0$  are shown in 4 and Fig. 5.

Fig. 4 shows the spin structure factor

$$\mathcal{S}(\mathbf{q}) = \sum_{ij} \langle \mathbf{S}_i(-\mathbf{q}) \cdot \mathbf{S}_j(\mathbf{q}) \rangle \quad (25)$$

in the plane  $\mathbf{q} = (h, h, l)$ . The structure factor is shown for two temperatures  $\frac{T}{J} = 5$  and  $\frac{T}{J} = 2$  for  $\theta = \frac{-11\pi}{16}$  (close to the “non-breathing” limit  $J_A = J_B$ ) and  $\theta = \frac{-9\pi}{16}$  (close to the isolated tetrahedra limit  $J_A = 0$ ). Fig. 5 shows the angle inte-

gral of Eq. (25), for the same sets of exchange parameters and a range of temperatures, as would be measured in a neutron scattering experiment on a powder sample

$$S_{\text{pow}}(Q) = \frac{1}{4\pi} \int d\theta d\phi \sin(\theta) \mathcal{S}(\mathbf{q}) \quad (26)$$

$$\mathbf{q} = Q(\sin(\theta) \cos(\phi), \sin(\theta) \sin(\phi), \cos(\theta)) \quad (27)$$

In both cases there is a sharpening of the scattering around into peaks around  $\mathbf{q} = (0, 0, 0)$  (and other Brillouin zone centers associated with ferromagnetic Bragg peaks) as the temperature approaches the ordering temperature  $T_{\text{FM}}$ . Within the SCGA this transition occurs when  $\lambda(T) = 0$ . Since the SCGA includes unphysical fluctuations which modulate the spin length, the resulting estimate of the transition temperature is likely to be an underestimate of the true transition temperature.

The sharpening of the scattering is less pronounced (for equal temperature) where the exchange parameters are closer to the isolated tetrahedra limit  $J_A = 0$ . In essence, where there is a large disparity between  $J_A$  and  $J_B$  the correlation length is limited by the weaker of the two exchange parameters.

This can be understood quantitatively by considering the behaviour of the ferromagnetic correlation length, obtained by expanding the SCGA calculation of Eq. (25) around  $\mathbf{q} = (0, 0, 0)$ . For this purpose, and for the calculations in Sections 4 and 5, we will set the ratio of bond lengths on the tetrahedra [Fig. 1] equal to unity

$$\frac{d_A}{d_B} = 1. \quad (28)$$

This assumption makes the analysis more transparent, and is not unphysical since in the real breathing pyrochlore materials  $\frac{d_A}{d_B}$  is very close to unity, e.g. 0.95 in  $\text{LiInCr}_4\text{O}_8$ .<sup>30</sup> Where we come to compare our calculations to experiments on  $\text{LiInCr}_4\text{O}_8$  in Section 6 we restore the true value of  $\frac{d_A}{d_B}$ .

In the region approaching  $\mathbf{q} = (0, 0, 0)$  we have

$$\mathcal{S}(\mathbf{q}) = \frac{6}{\lambda(T)} \left( \frac{1}{1 + \xi_{\text{eff}}^2} \right) + \mathcal{O}(q^4). \quad (29)$$

The square of the ferromagnetic correlation length  $\xi_{\text{eff}}^2$  may be written as the sum of two terms, with different behaviours approaching the ordering transition

$$\xi_{\text{eff}}^2 = \xi_0^2 + \xi_{\text{FM}}^2. \quad (30)$$

These two terms are

$$\xi_0^2 = \left( \frac{a_0}{4} \right)^2 \frac{\beta |J_A + J_B|}{2(\lambda(T) + 2\beta |J_A + J_B|)} \quad (31)$$

$$\xi_{\text{FM}}^2 = \left( \frac{a_0}{4} \right)^2 \frac{4\beta^2 J_A J_B \lambda(T)}{\lambda(T)^2 (\lambda(T) + 2\beta |J_A + J_B|)} \quad (32)$$

where  $a_0$  is the cubic lattice parameter of the breathing pyrochlore lattice.

Approaching the ordering transition at  $T = T_{\text{FM}}$ , we have

$$\lim_{T \rightarrow T_{\text{FM}}} \lambda(T) = 0. \quad (33)$$

In this limit the correlation length  $\xi_0$  saturates to a length scale of the order of the nearest neighbour distance

$$\lim_{\lambda \rightarrow 0} \xi_0(\lambda)^2 = \frac{a_0^2}{8}. \quad (34)$$

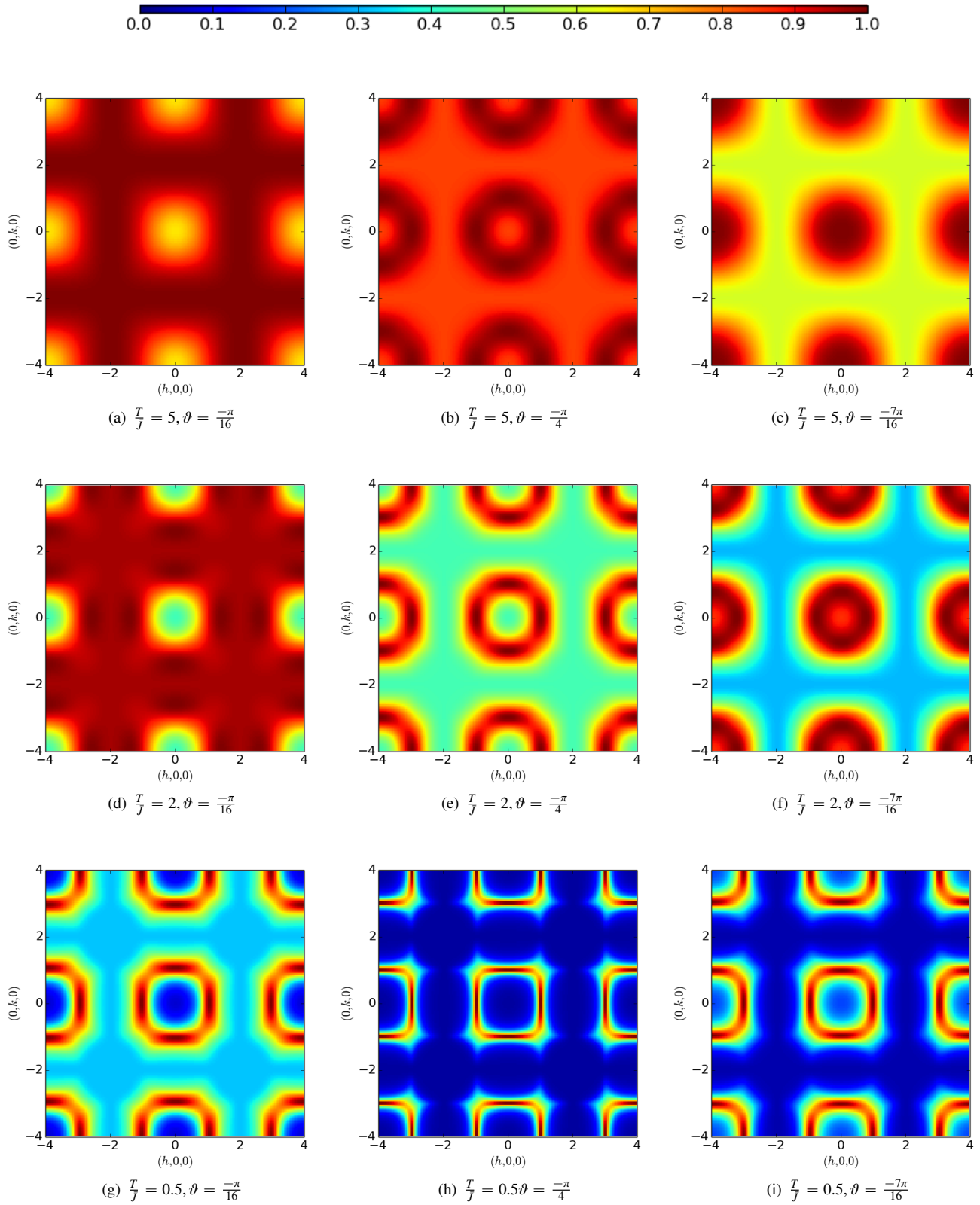


**Fig. 6.** (Color online) Spin structure factor  $S(\mathbf{q})$  [Eq. (25)] for  $\mathcal{H}_{\text{breathing}}$  [Eq. (1)] in the region of the phase diagram [Fig. 2] where  $J_A$  and  $J_B$  have opposite signs, in the plane  $\mathbf{q} = (h, k, 0)$ . For all values of  $\vartheta$  in this region the correlations evolve towards a “square ring” pattern, which comes from intersecting lines of soft modes with wavevectors of the form  $\mathbf{q} = (1, \delta, 0)$

Meanwhile the correlation length  $\xi_{FM}$  diverges as  $\frac{1}{\lambda}$

$$\lim_{\lambda \rightarrow 0} \xi_{FM}(\lambda)^2 = \left(\frac{a_0}{4}\right)^2 \frac{4\beta^2 J_A J_B \lambda(T)}{\lambda(T)^2 2\beta |J_A + J_B|} \sim \frac{1}{\lambda}. \quad (35)$$

Therefore as  $T \rightarrow T_{FM}$  we have

$$\xi_{FM}^2 \gg \xi_0^2 \implies \xi_{\text{eff}} \approx \xi_{FM} \quad (36)$$

In the high temperature limit  $\beta \rightarrow 0$  we have

$$\lim_{\beta \rightarrow 0} \xi_0^2 = \left(\frac{a_0}{4}\right)^2 \frac{\beta |J_A + J_B|}{2} \sim \beta \quad (37)$$

$$\lim_{\beta \rightarrow 0} \xi_{FM}^2 = \left(\frac{a_0}{4}\right)^2 \frac{4\beta^2 J_A J_B}{\lambda(T)} \sim \beta^2 \quad (38)$$

and so at high temperatures we have

$$\xi_0^2 \gg \xi_{FM}^2 \implies \xi_{\text{eff}} \approx \xi_0 \quad (39)$$

Seen in this light, the two correlation lengths  $\xi_0$  and  $\xi_{FM}$  are a quantitative measure of the extent to which the system may be thought of as a set of isolated tetrahedra. The crossover from the high temperature limit described by Eq. (39) to the strongly correlated regime described by Eq. (36) is a thermal crossover from the physics of isolated tetrahedra to the physics of a long-range correlated ferromagnet. The relative magnitudes of  $\xi_0$  and  $\xi_{FM}$  give a criterion for deciding whether a given ferromagnetic breathing pyrochlore at a given temperature is in the ‘‘isolated tetrahedron’’ limit.

When either  $J_A$  or  $J_B$  vanishes,  $\xi_{FM}$  also vanishes for all temperatures, since the system is then exactly described by a set of isolated tetrahedra.

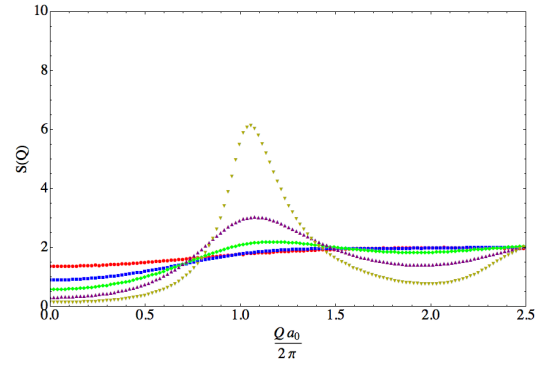
#### 4. $J_A$ and $J_B$ with opposite signs: dimensional reduction and order by disorder

We now turn to discuss the case where  $J_A$  and  $J_B$  have opposite signs. For concreteness we will take throughout this section

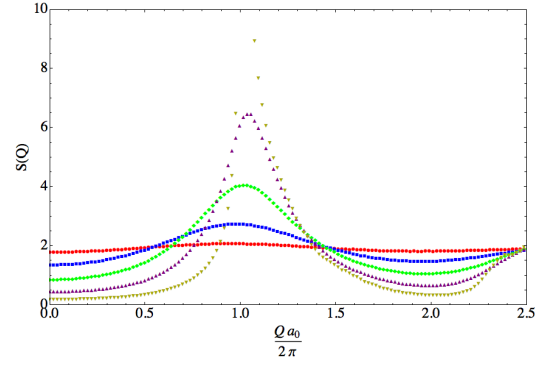
$$J_A > 0, \quad J_B < 0. \quad (40)$$

As discussed in Section 2, the ground state manifold in this case has a degeneracy of  $\mathcal{O}(L)$ , with states in the ground state manifold having associated wavevectors of the form  $\mathbf{q}_\delta = (1, 0, \delta)$ . At some finite temperature  $T_{\text{odd}}$  the system will order via the order-by-disorder mechanism. The relationship between this model and the classical antiferromagnet on the FCC lattice [Eq. (11)] suggests that this will occur via a first-order phase transition<sup>51</sup> and that the resulting ordered state will have wavevector  $\mathbf{q}_{\text{ord}} = (1, 0, 0)$  (or those related by symmetry).

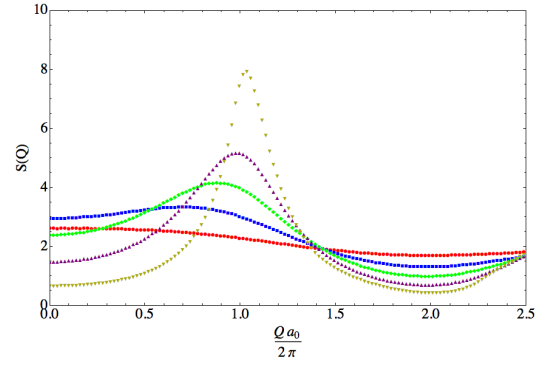
The development of these correlations in the plane  $\mathbf{q} = (h, k, 0)$  as a function of temperature and  $\vartheta$  [Eq. (2)] is shown in Fig. 6, for  $\vartheta = -\frac{\pi}{16}, -\frac{\pi}{4}, -\frac{7\pi}{16}$ . In all cases, the scattering develops with decreasing temperature towards the ‘‘square ring’’ pattern visible in Figs. 6 (g)-(i), which is formed from intersecting lines of scattering associated with the soft modes at  $\mathbf{q}_\delta = (1, \delta, 0)$ , modulated by a zone dependent form factor. These bright lines of scattering signal an effective decoupling of neighbouring [001] planes- which is somewhat reminiscent of the dimensional reduction observed in the rare-earth pyrochlore  $\text{Yb}_2\text{Ti}_2\text{O}_7$ .<sup>41,42,45</sup> In that system neighbouring [111] planes become effectively decoupled and the consequence is rods of scattering along the  $(h, h, h)$  directions of re-



(a)  $\vartheta = -\frac{\pi}{16}$ ;  $\frac{T}{J} = 5$  (●),  $\frac{T}{J} = 2$  (■),  $\frac{T}{J} = 1$  (◆),  $\frac{T}{J} = 0.5$  (▲),  $\frac{T}{J} = 0.2$  (▼)



(b)  $\vartheta = -\frac{\pi}{4}$ ;  $\frac{T}{J} = 5$  (●),  $\frac{T}{J} = 2$  (■),  $\frac{T}{J} = 1$  (◆),  $\frac{T}{J} = 0.5$  (▲),  $\frac{T}{J} = 0.2$  (▼)



(c)  $\vartheta = -\frac{7\pi}{16}$ ;  $\frac{T}{J} = 5$  (●),  $\frac{T}{J} = 2$  (■),  $\frac{T}{J} = 1$  (◆),  $\frac{T}{J} = 0.5$  (▲),  $\frac{T}{J} = 0.2$  (▼)

**Fig. 7.** (Color online) Angle integrated structure factor  $S_{\text{pow}}(Q)$  [Eq. (27)] for  $\mathcal{H}_{\text{breathing}}$  [Eq. (1)] in the region of the phase diagram [Fig. 2] where  $J_A$  and  $J_B$  have opposite signs. At high temperatures, correlations are limited to single tetrahedra and are ferromagnetic or antiferromagnetic depending on the sign of the dominant exchange parameter. At low temperatures these correlations evolve into an increasingly sharp peak near  $\frac{Qa_0}{2\pi} = 1$ , which is the result of antiferromagnetic correlations between internally ferromagnetic tetrahedra. The peak near  $\frac{Qa_0}{2\pi} = 1$  comes from integrating the square ring structure seen in Fig. 6 (g)-(i).

ciprocal space. Here, the rods are along the  $(1, 0, h)$  directions and are modulated by a zone dependent form factor resulting in the square ring structure.

In the case  $\vartheta = -\frac{\pi}{4}$  [Figs. 6 (b), (e), (h)], where  $|J_A| = |J_B|$  the scattering is only very weakly  $\mathbf{q}$  dependent at  $\frac{T}{J} = 5$ . This reflects an effect by which the frustration arising from the opposite exchange parameters, effectively reduces the temperature at which appreciable  $\mathbf{q}$  dependence in the correlations



arises. The “square ring” structure arises smoothly out of this, becoming increasingly sharp as the temperature is lowered.

In the case  $\vartheta = \frac{-\pi}{16}$  [Figs. 6 (a), (d), (g)], the antiferromagnetic  $J_A$  has a much larger magnitude than the ferromagnetic  $J_B$ . The high temperature correlations therefore simply reflect antiferromagnetic nearest-neighbour correlations on the  $A$  tetrahedra, with a broad minimum around  $\mathbf{q} = (0, 0, 0)$  and a broad minimum at the neighbouring Brillouin zone centers (e.g.)  $\mathbf{q} = (2, 0, 0)$ .

At a finite temperature  $T_{\text{ring}}^{\text{AFM}}$ , given by the equation

$$T_{\text{ring}}^{\text{AFM}} \lambda(T_{\text{ring}}^{\text{AFM}}) = \frac{-6J_B(6J_A - 2J_B)}{J_A + J_B} \quad (41)$$

the maximum at zone centers neighbouring the first Brillouin zone (e.g.  $\mathbf{q} = (2, 0, 0)$ ) inverts into a minimum, and a set of continuous set of maxima appear between  $\mathbf{q} = (0, 0, 0)$  and the neighbouring Brillouin zone centers. This set of maxima evolves into the “square ring” feature seen at low temperature. This temperature evolution of the correlations can be seen in angle integrated scattering shown in Fig. 7(a), where at broad maximum centred at

$$\frac{Qa_0}{2\pi} = 2$$

at high temperature turns into a minimum, with an increasingly sharp peak evolving towards

$$\frac{Qa_0}{2\pi} \approx 1.$$

The peak in the powder integral always retains a finite width and is shifted slightly to the right of  $\frac{Qa_0}{2\pi} = 1$  because it has a contribution from all wavevectors of the form  $\mathbf{q} = (1, 0, \delta)$ .

A similar picture describes the scattering when the ferromagnetic exchange parameter dominates the antiferromagnetic one. This is the case when  $\vartheta = \frac{-7\pi}{16}$  [Figs. 6 (c), (f), (i)]. Here the high temperature data has a broad maximum at  $\mathbf{q} = (0, 0, 0)$  reflecting ferromagnetic nearest neighbour correlations on the  $B$  tetrahedra. This maximum inverts at a temperature given by

$$T_{\text{ring}}^{\text{FM}} \lambda(T_{\text{ring}}^{\text{FM}}) = \frac{J_A(6J_B - 2J_A)}{J_A + J_B} \quad (42)$$

and a continuous set of maxima appear which evolve towards the “square ring” feature seen at low temperature. The same evolution can be seen in the powder integrated scattering in Fig. 7(c).

It is interesting to note that a “square ring” feature, rather similar to that seen in Fig. 6 has also been seen in reverse Monte Carlo reconstructions of the scattering from the double perovskite material  $\text{Ba}_2\text{YRuO}_6$  in which the  $\text{Ru}^{5+}$  ions form an FCC lattice.<sup>52</sup> This material orders into  $\mathbf{q} = (1, 0, 0)$  antiferromagnetic state shown in Fig. 3(b) below  $T = 36\text{K}$ .

### 5. $J_A > 0, J_B > 0$ : Coulombic spin liquid

We now turn to discuss the spin correlations in the antiferromagnetic region of the phase diagram where the system enters a Coulomb phase at low temperature. These are shown for  $\vartheta = \frac{\pi}{16}$  and  $\vartheta = \frac{3\pi}{16}$  in Fig. 8 and Fig. 9.

The onset of the classical Coulomb phase is signalled by the sharpening of bow-tie like “pinch point” features around reciprocal lattice vectors such as  $\mathbf{q} = (0, 0, 2)$ . In the  $T \rightarrow 0$  limit these features become sharp singularities<sup>13,14</sup> but at fi-

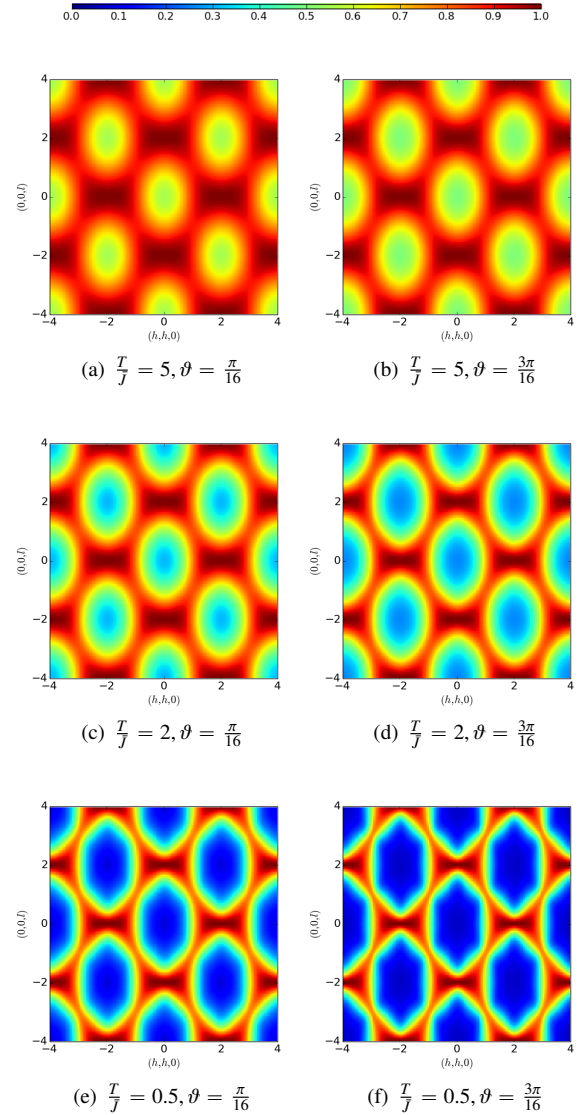


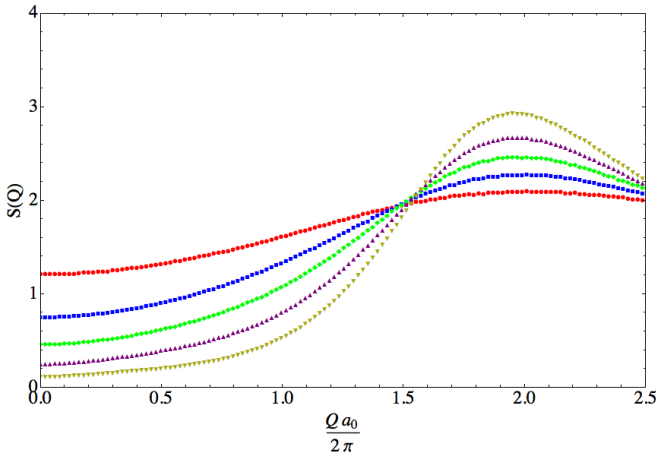
**Fig. 8.** (Color line) Spin structure factor  $S(\mathbf{q})$  [Eq. (25)] in the antiferromagnetic (Coulomb phase) region of the phase diagram [Fig. 2] of  $\mathcal{H}_{\text{breathing}}$  [Eq. (1)], shown for  $\vartheta = \frac{\pi}{16}$  and  $\vartheta = \frac{3\pi}{16}$ . With decreasing temperature, bow-tie-like pinch point structures appear near certain Brillouin zone centers, e.g.  $\mathbf{q} = (0, 0, 2)$ . As  $T \rightarrow 0$  these become sharp singularities. At finite temperature the singularity is cut off by a correlation length  $\xi_{\parallel}$ , which diverges as  $T^{-1/2}$ , signalling the onset of algebraic ( $\sim r^{-3}$ ) correlations in real space. The divergent part of the correlation length is proportional to the product  $J_A J_B$  and therefore the development of the correlations is slower when closer to the isolated tetrahedron limit.

nite temperature they have a finite width in the longitudinal direction  $\xi_{\parallel}^{-1}$ . The length scale  $\xi_{\parallel}$  cuts off the algebraic real space correlations at long distances, reverting them to an exponential form for  $r \gg \xi_{\parallel}$ . As  $T \rightarrow 0$ ,  $\xi_{\parallel}$  diverges as  $T^{-1/2}$  and the correlations are algebraic out to infinite separation.

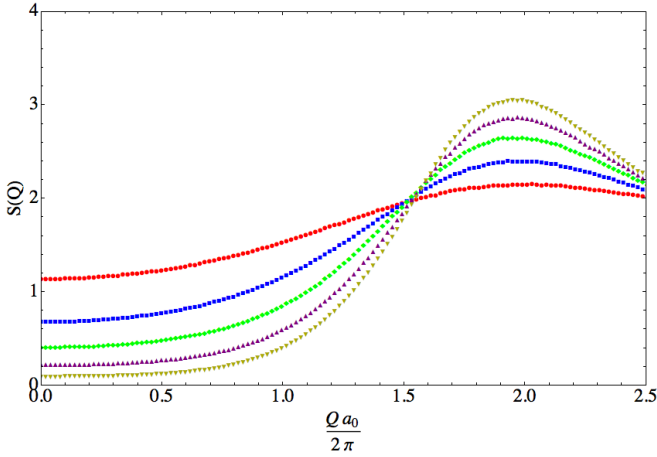
We may understand this crossover in the breathing pyrochlore case, by calculating  $\xi_{\parallel}$  as a function of  $J_A, J_B$  and  $T$  within the SCGA. This is done by expanding the SCGA prediction for  $S(\mathbf{q})$  around  $(0, 0, 2)$ . We find

$$S((0, 0, 2 + \tilde{q})) \approx \frac{6}{\lambda(T)} \left( \frac{1}{1 + \xi_{\parallel}^2 \tilde{q}^2} \right) + O(\tilde{q}^4). \quad (43)$$

The square of the correlation length  $\xi_{\parallel}^2$  may be written as a sum of two terms, one of which reflects single tetrahe-



(a)  $\vartheta = \frac{\pi}{16}$ ;  $\frac{T}{J} = 5$  (●),  $\frac{T}{J} = 2$  (■),  $\frac{T}{J} = 1$  (◆),  $\frac{T}{J} = 0.5$  (▲),  $\frac{T}{J} = 0.2$  (▼)



(b)  $\vartheta = \frac{3\pi}{16}$ ;  $\frac{T}{J} = 5$  (●),  $\frac{T}{J} = 2$  (■),  $\frac{T}{J} = 1$  (◆),  $\frac{T}{J} = 0.5$  (▲),  $\frac{T}{J} = 0.2$  (▼)

**Fig. 9.** (Color online) Angle integrated structure factor  $S_{\text{pow}}(\mathbf{q})$  [Eq. (27)] in the Coulombic spin liquid phase of  $\mathcal{H}_{\text{breathing}}$  [Eq. (1)]. Correlations are shown for  $\vartheta = \frac{\pi}{16}$  and  $\vartheta = \frac{3\pi}{16}$  [cf. Fig. 2]. The development of sharp pinch point features, as seen in Fig. 8, is hidden by the angular integration and the powder structure factor shows a growing, broad peak near  $\frac{Qa_0}{2\pi}$ . This is consistent with experimental observations on the breathing pyrochlore  $\text{LiInCr}_4\text{O}_8$  as discussed in Section 6 and shown in Fig. 10.

dron correlations and dominates at high temperature the other of which reflects the correlations of the Coulomb phase and dominates at low temperature

$$\xi_{\parallel}^2 = \xi_0^2 + \xi_{\text{Coulomb}}^2 \quad (44)$$

$$\xi_0^2 = \left(\frac{a_0}{4}\right)^2 \left(\frac{2\beta\lambda(T)(J_A + J_B)}{4\lambda(T)^2 + 8\beta\lambda(T)(J_A + J_B)}\right) \quad (45)$$

$$\xi_{\text{Coulomb}}^2 = \left(\frac{a_0}{4}\right)^2 \left(\frac{16\beta^2 J_A J_B}{4\lambda(T)^2 + 8\beta\lambda(T)(J_A + J_B)}\right) \quad (46)$$

In the spin liquid region of the phase diagram the Lagrange multiplier  $\lambda(T)$  tends to a finite value at both high and low temperature. Thus, in the low temperature limit we have

$$\lim_{T \rightarrow 0} \xi_0^2 = \left(\frac{a_0}{8}\right)^2 \quad (47)$$

$$\lim_{T \rightarrow 0} \xi_{\text{Coulomb}}^2 = \left(\frac{a_0}{4}\right)^2 \left(\frac{2\beta J_A J_B}{\lambda(T)(J_A + J_B)}\right) \sim \frac{1}{T}$$

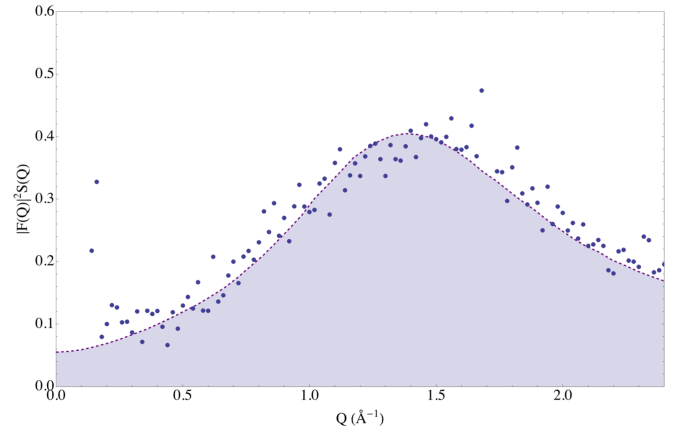


**Fig. 10.** (Color online) Comparison of SCGA calculations with experimental neutron scattering data<sup>32</sup> for a powder sample of for  $\text{LiInCr}_4\text{O}_8$  at  $T = 30\text{K}$ . The lattice constant  $a_0 = 8.42\text{\AA}$  and the bond lengths  $d_A = 2.903\text{\AA}$  and  $d_B = 3.052\text{\AA}$  are set to their experimental values.<sup>30</sup> The exchange constants are taken from an estimate by Okamoto *et al.* based on an empirical relationship between the bond lengths and the exchange parameters in Cr spinels:<sup>30</sup>  $J_A = 60\text{K}$  and  $J_B = 6\text{K}$ . The SCGA calculation of the scattering has been multiplied by the form factor for  $\text{Cr}^{3+}$  ions  $|F(Q)|^2$ . There is one adjustable parameter in the comparison which is a multiplicative scale factor setting the overall normalisation. The agreement is very good, which suggests that the estimated exchange parameters are approximately correct in this temperature range and underlines the validity of the SCGA description in the paramagnetic, cubic symmetry phase of  $\text{LiInCr}_4\text{O}_8$ .

$$(48)$$

$$\xi_0^2 \ll \xi_{\text{Coulomb}}^2 \implies \xi_{\parallel} \approx \xi_{\text{Coulomb}} \sim T^{-1/2} \quad (49)$$

and the correlation length diverges as  $T^{-1/2}$  as expected for a Coulomb phase. In the case  $J_A = J_B$  these expressions reproduce the results of Conlon and Chalker.<sup>49</sup>

In the high temperature limit we have

$$\lim_{\beta \rightarrow 0} \xi_0^2 = \left(\frac{a_0}{4}\right)^2 \left(\frac{2\beta(J_A + J_B)}{4\lambda(T)}\right) \sim \beta \quad (50)$$

$$\lim_{\beta \rightarrow 0} \xi_{\text{Coulomb}}^2 = \left(\frac{a_0}{4}\right)^2 \left(\frac{16\beta^2 J_A J_B}{4\lambda(T)^2}\right) \sim \beta^2 \quad (51)$$

$$\xi_{\text{Coulomb}}^2 \ll \xi_0^2 \implies \xi_{\parallel} \approx \xi_0 \quad (52)$$

and the correlations are essentially described by a model of isolated tetrahedra. Comparison of the length scales  $\xi_{\text{Coulomb}}$  and  $\xi_0$  gives a criterion to define the thermal crossover from isolated tetrahedron correlations to isolated Coulomb phase correlations in an antiferromagnetic breathing pyrochlore.

In the powder structure factor shown in Fig. 9 the sharpness of the pinch point features is hidden by the angular integration [Eq. (27)] and the scattering simply shows a broad maximum around

$$\frac{Qa_0}{2\pi} = 2. \quad (53)$$

This maximum grows in intensity and becomes sharper with decreasing temperature but remains always rather broad due to the angular integration. This is consistent with neutron scattering experiments on  $\text{LiInCr}_4\text{O}_8$ , as will be discussed further in Section 6.

## 6. Discussion

In this article we have considered the minimal model for magnetism on the breathing pyrochlore lattice [Eq. (1)]. We have seen that the ground state manifold depends only on the signs of the two exchange couplings, associated with the two species of tetrahedra [Section 2]. The classical ground state phase diagram [Fig. 2] contains a ferromagnetic phase (for  $J_A < 0, J_B < 0$ ) a disordered Coulomb phase (for  $J_A > 0, J_B > 0$ ) and a phase where an  $O(L)$  degeneracy is lifted by the order-by-disorder mechanism (for  $J_A > 0, J_B < 0$  or vice versa). The temperature development of the spin correlations in each case is calculated using the Self Consistent Gaussian Approximation (SCGA)<sup>46–49</sup> and is discussed for each region of the phase diagram in Sections 3–5.

At this point it is interesting to compare our calculations with the results of the recent neutron scattering experiments by Okamoto *et al.*<sup>32</sup> These authors measured the neutron scattering response of powder samples of breathing pyrochlores  $\text{LiIn}_x\text{Ga}_{1-x}\text{Cr}_4\text{O}_8$ . Their neutron scattering data for  $x = 1$  (i.e. for  $\text{LiInCr}_4\text{O}_8$ ) at  $T = 30\text{K}$ , are shown in Fig. 10.

In Ref. 30 the authors provided an estimate of the exchange parameters for  $\text{LiInCr}_4\text{O}_8$ , based on an empirical relationship between the exchange parameters and the bond distances, obtaining

$$J_A = 60\text{K}, \quad J_B = 6\text{K}. \quad (54)$$

We have compared the results of our SCGA calculation using this parameter set with the neutron scattering data from Ref. 32. The result is shown in Fig. 10. The comparison shows very good agreement, with one adjustable parameter which is a multiplicative scale factor setting the overall normalisation. This suggests that the exchange parameters proposed in Ref. 30 [Eq. (54)] are at least approximately correct, at temperatures above the structural transition and underlines the validity of the description presented here. If we fix the overall energy scale  $\bar{J} = \sqrt{J_A^2 + J_B^2}$  [Eq. (2)] and vary the ratio  $\frac{J_B}{J_A}$  we find that reasonably good agreement is obtained for the range of values

$$0.05 \lesssim \frac{J_B}{J_A} \lesssim 0.15. \quad (55)$$

Rather surprisingly, we are unable to obtain a convincing fit to the higher temperature data at  $T = 150\text{K}$ . As noted by the authors of Ref. 32, the experimental scattering at  $T = 150\text{K}$  is simply form-factor like, suggesting vanishing spin correlations, whereas our analysis predicts measurable nearest-neighbour spin correlations at  $T = 150\text{K}$  for the estimated  $J_A = 60\text{K}$  and  $J_B = 6\text{K}$ . If we allow  $J_A$  and  $J_B$  to vary, we are unable to obtain any parameter set which simultaneously describes the data at both temperatures.

This may be an indication that coupling to the lattice gives rise to an effectively temperature dependent exchange energy scale. This seems plausible since the dominant exchange pathway is direct exchange between  $\text{Cr}^{3+}$  ions, which is highly sensitive to the Cr-Cr distance.<sup>36</sup>

In conclusion, the recently synthesized breathing pyrochlore materials offer new opportunities in the study of frustrated magnetism, playing host to spin-liquid and order-by-disorder physics. It may be particularly interesting for future experimental studies to investigate sulfide and selenide

breathing pyrochlores<sup>53</sup> which could potentially realise the case of opposite exchange parameters discussed in Section 4, which exhibits an unusual structure of spin correlations and order-by-disorder.

The determination of the full phase diagram of  $\mathcal{H}_{\text{breathing}}$  [Eq. (1)] in the presence of quantum fluctuations remains an important and interesting open question. Moreover, experimental results on the breathing pyrochlores  $\text{LiInCr}_4\text{O}_8$  and  $\text{LiGaCr}_4\text{O}_8$  make it evident that the effect of coupling to the lattice is an important direction for future work.<sup>30–33</sup> We expect that as in the “non-breathing” case,<sup>16,17,20</sup> the physics uncovered by a treatment of the spin-lattice coupling will be very rich indeed.

## Acknowledgements

We thank Zenji Hiroi, Gøran Nilsen and Yoshihiko Okamoto for discussions about experiments, for helpful comments on the manuscript and for sharing the neutron scattering data from Ref. 32, shown in Fig. 10. This work was supported by the Theory of Quantum Matter unit of the Okinawa Institute of Science and Technology Graduate University

- 1) P. A. Lee, *Science*, **321**, 1306, (2008).
- 2) L. Balents, *Nature* **464**, 199, (2010).
- 3) C. Castelnovo, R. Moessner and S. L. Sondhi, *Nature* **451**, 42, (2008).
- 4) T. Fennell, P. P. Deen, A. R. Wildes, K. Schmalzl, D. Prabhakaran, A. T. Boothroyd, R. J. Aldus, D. F. McMorrow and S. T. Bramwell, *Science* **326**, 415, (2009).
- 5) M. Yamashita, N. Nakata, Y. Kasahara, T. Sasaki, N. Yoneyama, N. Kobayashi, S. Fujimoto, T. Shibauchi and Y. Matsuda, *Nature Phys.* **5**, 44, (2009).
- 6) T. H. Han, J. S. Helton, S. Y. Chu, D. G. Nocera, J. A. Rodriguez-Rivera, C. Broholm and Y. S. Lee, *Nature* **492**, 406, (2012)
- 7) K. Kimura, S. Nakatsuji, J.-J. Wen, C. Broholm, M. B. Stone, E. Nishibori and H. Sawa, *Nature Commun.* **4**, 1934 (2013).
- 8) M. Hirschbinger, J. W. Krizan, R. J. Cava and N. P. Ong, *Science* **348**, 106, (2015).
- 9) J. S. Gardner, M. J. P. Gingras and J. E. Greedan, *Rev. Mod. Phys.* **82**, 53, (2010).
- 10) J. N. Reimers, A. J. Berlinsky and A. C. Shi, *Phys. Rev. B* **43**, 865, (1991).
- 11) R. Moessner and J. T. Chalker, *Phys. Rev. Lett.* **80**, 2929, (1998).
- 12) R. Moessner and J. T. Chalker, *Phys. Rev. B* **58**, 12049, (1998).
- 13) S. V. Isakov, K. Gregor, R. Moessner and S. L. Sondhi, *Phys. Rev. B* **93**, 167204, (2004).
- 14) C. L. Henley, *Annu. Rev. Condens. Matter Phys.* **1**, 179, (2010).
- 15) C. Castelnovo, R. Moessner and S. L. Sondhi, *Annu. Rev. Condens. Matter Phys.* **3**, 35, (2012).
- 16) Y. Yamashita and K. Ueda, *Phys. Rev. Lett.* **85**, 4960, (2000).
- 17) O. Tchernyshyov, R. Moessner and S. L. Sondhi, *Phys. Rev. Lett.* **88**, 067203, (2002).
- 18) S. Ji, S.-H. Lee, C. Broholm, T. Y. Koo, W. Ratcliff, S.-W. Cheong and P. Zschack, *Phys. Rev. Lett.* **103**, 037201, (2009).
- 19) H. Ueda, H. Mitamura, T. Goto and Y. Ueda, *Phys. Rev. B* **73**, 094415, (2006).
- 20) K. Penc, N. Shannon and H. Shiba, *Phys. Rev. Lett.* **93**, 197203, (2004).
- 21) N. Shannon, H. Ueda, Y. Motome, K. Penc and H. Takagi, *J. Phys.: Conf. Series* **51**, 31, (2006).
- 22) K. Penc, N. Shannon, Y. Motome and H. Shiba, *J. Phys.: Condens. Matter* **19**, 145267 (2007).
- 23) Y. Motome, K. Penc and N. Shannon, *J. Magn. Magn. Mater.* **300**, 57, (2006).
- 24) N. Shannon, K. Penc and Y. Motome, *Phys. Rev. B* **81**, 184409, (2010).
- 25) H. Ueda, H. A. Katori, H. Mitamura, T. Goto and H. Takagi, *Phys. Rev. Lett.* **94**, 047202, (2005).
- 26) E. Kojima, A. Miyata, S. Miyabe, S. Takeyama, H. Ueda and Y. Ueda,

- Phys. Rev. B **77**, 212408, (2008).
- 27) A. Miyata, H. Ueda, Y. Ueda, H. Sawabe and S. Takeyama, Phys. Rev. Lett. **107**, 207203, (2011).
- 28) A. Miyata, H. Ueda, Y. Ueda, Y. Motome, N. Shannon, K. Penc and S. Takeyama, J. Phys. Soc. Jpn. **80**, 074709, (2011).
- 29) A. Miyata, H. Ueda, Y. Ueda, Y. Motome, N. Shannon, K. Penc and S. Takeyama, J. Phys. Soc. Jpn **81**, 114701, (2012).
- 30) Y. Okamoto, G. J. Nilsen, J. P. Attfield and Z. Hiroi, Phys. Rev. Lett. **110**, 097203, (2013).
- 31) Y. Tanaka, M. Yoshida, M. Takigawa, Y. Okamoto and Z. Hiroi, Phys. Rev. Lett. **113**, 227204, (2014).
- 32) Y. Okamoto, G. J. Nilsen, T. Nakazono and Z. Hiroi, J. Phys. Soc. Jpn. **84**, 043707 (2015).
- 33) G. J. Nilsen, Y. Okamoto, T. Masuda, J. Rodriguez-Carvajal, H. Mutka, T. Hansen, and Z. Hiroi, Phys. Rev. B **91**, 174435 (2015)
- 34) K. Kimura, S. Nakatsuji and T. Kimura, Phys. Rev. B **90**, 060414(R), (2014).
- 35) A. Yaresko and V. Antonov, J. Magn. Magn. Mater. **310**, 1672, (2007).
- 36) A. Yaresko, Phys. Rev. B **77**, 115106, (2008).
- 37) A. B. Harris, A. J. Berlinsky and C. Bruder, J. Appl. Phys. **69**, 5200, (1991).
- 38) B. Canals and C. Lacroix, Phys. Rev. Lett. **80**, 2933, (1998).
- 39) B. Canals and C. Lacroix, Phys. Rev. B **61**, 1149, (2000).
- 40) H. Tsunetsugu, J. Phys. Soc. Jpn. **70**, 640, (2001).
- 41) K. A. Ross, J. P. C. Ruff, C. P. Adams, J. S. Gardner, H. A. Dabkowska, Y. Qiu, J. R. D. Copley and B. D. Gaulin, Phys. Rev. Lett. **103**, 227202, (2009).
- 42) K. A. Ross, L. R. Yaraskavitch, M. Laver, J. S. Gardner, J. A. Quilliam, S. Meng, J. B. Kycia, D. K. Singh, Th. Proffen, H. A. Dabkowska and B. D. Gaulin, Phys. Rev. B **84**, 174442, (2011).
- 43) L. Savary, K. A. Ross, B. D. Gaulin, J. P. C. Ruff and L. Balents, Phys. Rev. Lett. **109**, 167201, (2012).
- 44) M. E. Zhitomirsky, M. V. Gvozdikova, P. C. W. Holdsworth and R. Moessner, Phys. Rev. Lett. **109**, 077204, (2012).
- 45) H. Yan, O. Benton, L. D. C. Jaubert and N. Shannon, arXiv:1311.3501.
- 46) B. Canals and D. A. Garanin, Can. J. Phys. **79**, 1323, (2001).
- 47) T. S. Pickles, J. E. Saunders and J. T. Chalker, Europhys. Lett. **84**, 36002, (2008).
- 48) P. H. Conlon and J. T. Chalker, Phys. Rev. Lett. **102**, 237206, (2009).
- 49) P. H. Conlon and J. T. Chalker, Phys. Rev. B **81**, 22413, (2010).
- 50) C. L. Henley, J. Appl. Phys. **61**, 3962, (1987).
- 51) M. V. Gvozdikova and M. E. Zhitomirsky, JETP Lett. **81**, 236, (2005).
- 52) G. J. Nilsen, C. M. Thompson, G. Ehlers, C. Marjerrison and J. E. Greedan, Phys. Rev. B **91**, 054415, (2015).
- 53) H. L. Pinch, M. J. Woods and E. Lopatin, Mater. Res. Bull. **5**, 425, (1970).